The role of strain-induced structural changes in the metal–insulator transition in epitaxial $SmNiO_3$ films

2008 J. Phys.: Condens. Matter 20 145216

(http://iopscience.iop.org/0953-8984/20/14/145216)

J. Phys.: Condens. Matter **20** (2008) 145216 (7pp) doi:10.1088/0953-8984/20/14/145216

The role of strain-induced structural changes in the metal–insulator transition in epitaxial $SmNiO_3$ films

F Conchon[1,5], A Boulle[1], R Guinebretière[1], E Dooryhée[2], J-L Hodeau[2], C Girardot[3,4], S Pignard[3], J Kreisel[3] and F Weiss[3]

[1] Laboratoire Science des Procédés Céramiques et de Traitements de Surfaces (SPCTS), CNRS UMR 6638, ENSCI, 47 Avenue Albert Thomas, 87065 Limoges, France
[2] Institut Néel (IN), CNRS UPR 2940, 25 avenue des Martyrs BP 166, 38042 Grenoble, France
[3] Laboratoire des Matériaux et du Génie Physique (LMGP), CNRS UMR 5628, INP Grenoble, MINATEC, 3 parvis Louis Néel—BP 257, 38016 Grenoble, France
[4] Schneider Electric, 160 rue des Martyrs, 38000 Grenoble, France

E-mail: florineconchon@gmail.com

Received 13 December 2007, in final form 11 February 2008
Published 19 March 2008
Online at stacks.iop.org/JPhysCM/20/145216

Abstract

The present work is devoted to explaining the role of epitaxial strain in the structure and the metal–insulator (MI) transition in $SmNiO_3$ (SNO) films deposited on $LaAlO_3$ (LAO) and $SrTiO_3$ (STO) substrates. X-ray reciprocal space mapping and valence bond calculations allow us to show that in-plane compressive strain (for SNO/LAO) stabilizes Ni^{3+} in the orthorhombically distorted structure with the result that films exhibit a sharp MI transition at 120 °C, whereas in-plane tensile strain (for SNO/STO) stabilizes Ni^{2+}, implying the creation of oxygen vacancies, which is accompanied by a 'flattening' of the resistivity curves together with a huge increase of the overall resistivity. As SNO films are deposited on STO, we demonstrate that strain relaxation acts like the temperature or the rare-earth size, increasing the Ni–O–Ni bond angles. Hence in-plane tensile strain shifts the MI transition towards high temperatures. The flattening of the resistivity curve observed for SNO/STO can be understood by taking into account the inhomogeneous strain distribution across the film thickness (strain gradient) while the increase in resistivity has been ascribed to the homogeneous part of the strain.

(Some figures in this article are in colour only in the electronic version)

1. Introduction

$RNiO_3$ perovskites (R is a rare-earth) belong to the orthorhombically distorted perovskite family and have been extensively studied in the last few years since the report of the existence of a metal–insulator (MI) transition as a function of temperature [1, 2]. Associated with this MI transition, a small discontinuous decrease of the unit cell volume is observed as the temperature increases [3]. The occurrence of this thermally driven MI transition has been related to the gradual closing of the charge transfer gap between the oxygen 2p valence bond and the nickel 3d conduction band across the Fermi level due to thermal increase of the bandwidth [1, 4, 5].

Experimental evidence suggests that the critical temperature of the phase transition (T_{MI}) depends on the Ni–O–Ni bond angle. This angle is generally less than 180° because of the orthorhombic distortion which is conventionally discussed in terms of rare-earth size and tolerance factor [2]: $t = d(\text{R–O})/\sqrt{2} \times d(\text{Ni–O})$. If the rare-earth ion is large enough to give $t = 1$, the rare-earth–oxygen bond lengths, d(R–O), and nickel–oxygen bond lengths, d(Ni–O), are compatible with the ideal perovskite structure, i.e. with no orthorhombic distortion and an Ni–O–Ni bond angle equal to 180°. Since the rare-earth size is too small to satisfy this criterion, the structure becomes distorted as the NiO_6 octahedra tilt in order to fill the extra space which, in turn, gives rise to bent Ni–O–Ni angles determining the degree of overlapping of the Ni 3d and O 2p

[5] Author to whom any correspondence should be addressed.

bands [6]. As the size of the rare-earth increases (and hence the tolerance factor), the orthorhombic distortion decreases and the Ni–O–Ni bond angle straightens out then lowering T_{MI} and stabilizing the metallic state over the semi-conducting state. This can be achieved by increasing the rare-earth radius [2], by applying an external pressure [7, 8] or by using epitaxial strain [9, 10].

The stabilization in oxygen lattices of the highest oxidation states of transition metals is an important challenge for studying electronic phenomena in oxides [11]. For instance, the less stable 3+ oxidation state of Ni was stabilized in $RNiO_3$ using high oxygen pressures and high temperatures [12, 13]. Nevertheless, the presence of Ni^{3+} implies the possibility of large oxygen deficiency for $RNiO_3$ [14, 15]. To date, only few studies were devoted to analyze the effect of oxygen non-stoichiometry on the transport properties of $RNiO_3$ and all of them aimed to investigate bulk $RNiO_3$ [14–16]. In $SmNiO_{3-\delta}$ and $NdNiO_{3-\delta}$ ceramics, it has been observed that oxygen vacancies greatly influence the transport properties. For instance, according to Tiwari *et al* [15] the MI transition is strongly 'flattened' and T_{MI} increases as δ increases. However, the role played by oxygen vacancies is still not understood. Since epitaxial strain is used to stabilize the $RNiO_3$ phase, it can hence be expected that the misfit strain between the substrate and the film will also profoundly affect the structure and hence the MI transition of the epitaxial film. Up to now, the epitaxial stabilization mechanism of the $RNiO_3$ phases and more particularly the stabilization of Ni^{3+} and the consequence on the MI transition remain unclear. This paper addresses these two issues and is divided into two main sections which can be summarized as follows.

With the aid of high resolution x-ray diffraction (HRXRD), we will demonstrate using the particular example of $SmNiO_3$ (SNO) deposited on $SrTiO_3$ (STO) (in-plane tensile strain) and on $LaAlO_3$ (LAO) (in-plane compressive strain) that Ni^{3+} is stabilized in the $RNiO_3$ structure by an in-plane compressive strain whereas the in-plane tensile strain induces the formation of oxygen vacancies in the $RNiO_3$ structure and at the same time a strong 'flattening' of the MI transition together with a huge increase of the overall resistivity. Moreover, in the case of SNO films deposited on STO, we will evidence that the formation of oxygen vacancies reduces both the formal valence of nickel and the Ni–O–Ni bond angle and hence rises the MI transition temperature. Finally, upon careful analysis of the resistivity curves we will show that the flattened MI transition observed in the case of films deposited on STO can be ascribed to the existence of a strain gradient within the SNO films.

2. Experiment

SNO films were grown by an injection metal–organic chemical vapor deposition process [17] on single crystal (001) LAO and STO substrates. The epitaxial relationships between the SNO films and the substrates can be written as $(001)_{SNO} \parallel (001)_{STO} - [100]_{SNO} \parallel [100]_{STO}$ and $(001)_{SNO} \parallel (001)_{LAO} - [100]_{SNO} \parallel [100]_{LAO}$ [18]. With these orientations the misfit strain is defined as $e_0 = \frac{a_S - a^{th}_{SNO}}{a^{th}_{SNO}}$, where a_S and a^{th}_{SNO} are respectively the strain-free lattice parameters of the substrate and the film. With $a_{STO} = 3.905$ Å, $a_{LAO} = 3.789$ Å and $a^{th}_{SNO} = 3.795$ Å (in the pseudo-cubic notation), $e_0 = 2.89\%$ for SNO/STO and $e_0 = -0.13\%$ for SNO/LAO. Four-probe resistivity measurements were carried out in the temperature range 30–350 °C on a homemade setup. Finally, SNO films were characterized by HRXRD. For the purpose of analyzing strain in epitaxial films, x-ray diffraction, and in particular reciprocal space mapping, is a well-established reference technique [19–21]. A laboratory diffractometer ($\lambda_{Cu\ K\lambda 1} = 1.5406$ Å) equipped with a four reflection monochromator and a position sensitive detector was used to record asymmetrical $(\bar{1}03)$ reciprocal space maps (RSMs) [22] in the (H, L) plane, where H and L are the continuous Miller indices in the film plane and perpendicular to it, respectively. High resolution (002) L scans were carried out at the European Synchrotron Radiation Facility (ESRF, Grenoble—France) on the BM2 beam-line [23]. A single Si(111) crystal is used as an analyzing crystal. The wavelength was set to $\lambda = 0.613$ Å. $(\bar{1}03)$ RSMs and (002) L scans allowed us to assess the strain state as well as the structural features of the SNO films as a function of the strain relaxation rate.

The present study is primarily based on strain investigations especially by reciprocal space mapping. A careful analysis of the asymmetrical $(\bar{1}03)$ RSMs allows us to derive for each film the actual lattice parameter of SNO, a_{SNO}, as well as the mechanical and chemical strain relaxation rates, R_m and R_c, from the in-plane and out-of-plane strained lattice parameters of the films, $a_\parallel$ and $a_\perp$:

$$a_{SNO} = \frac{a_\perp + \nu_2 \times a_\parallel}{\nu_2 + 1} \tag{1}$$

where ν_2 [24] is defined as the ratio of the vertical strain $e_\perp$ to the lateral strain $e_\parallel$ and is equal to $2C_{12}/C_{11}$ and

$$R_m = \frac{a_\parallel - a_S}{a_{SNO} - a_S} \quad \text{and} \quad R_c = \frac{a_{SNO} - a^{th}_{SNO}}{a_S - a^{th}_{SNO}}. \tag{2}$$

For a fully strained film, $a_\parallel = a_S$ so that $R_m = 0$, which gives rise to the alignment of the film and substrate reciprocal lattice points (RLPs) along [001]. For a fully strain relaxed film $a_\parallel = a_{SNO}$ so that $R_m = 1$, which gives rise to the alignment of the film and the substrate RLPs [25] along $[\bar{1}03]$. The presence of the less stable 3+ oxidation state of the nickel implies large oxygen deficiency in $RNiO_3$ compounds. It can hence be expected that this oxygen deficiency will induce an effect on the lattice parameters and then on the global strain relaxation. We introduce R_c, i.e. the contribution of the chemical composition to the overall strain relaxation. In fact, the chemical strain relaxation corresponds to the reduction of the lattice strain due to the change in bulk lattice parameter of SNO (a_{SNO}). Indeed, as $a_{SNO} = a^{th}_{SNO}$ then $R_c = 0$ and the film/substrate lattice mismatch has its usual value (2.89%), whereas when $a_{SNO} = a_S$, then $R_c = 1$ and the film/substrate lattice mismatch obviously drops to 0. The remaining mismatch can then be relieved mechanically as given by R_m. Finally, using the above definitions, in

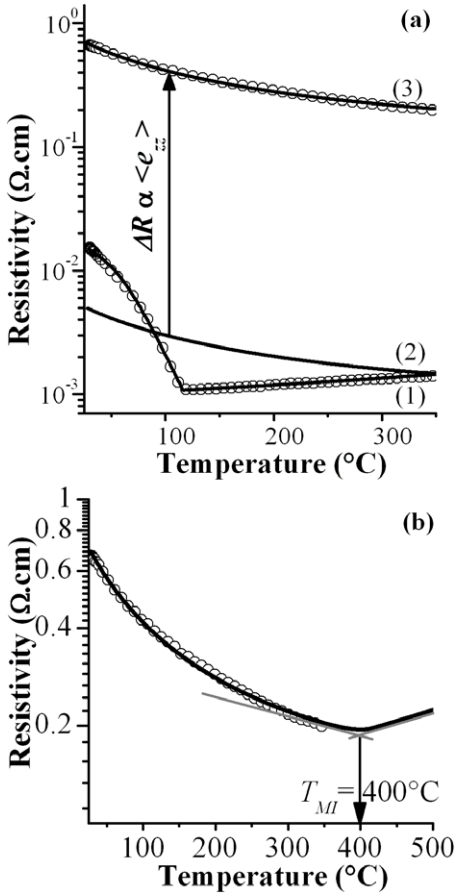

Figure 1. (a) Plot of the resistivity versus temperature of two 17 nm thick films. Curve 1 corresponds to SNO deposited on LAO (circles: data, line: calculation from equation (5)), curve 2 corresponds to the calculated resistivity curve considering that the film is divided into 20 lamellas (equation (6)): the distribution of T_{MI} across the film thickness results in a strong flattening of the resistivity curve. Curve 3 corresponds to SNO deposited on STO (circles: data, line: calculated curve from equation (6)). (b) Curve 3 plotted in the temperature range 30–500 °C, it clearly evidences a MI transition at $T_{\mathrm{MI}} = 400$ °C instead of 130 °C.

equations (1) and (2), the total strain relaxation in the film can be written:

$$R_{\mathrm{t}} = \frac{a_{\mathrm{S}} - a_{\parallel} + a_{\mathrm{SNO}} - a_{\mathrm{SNO}}^{\mathrm{th}}}{a_{\mathrm{S}} - a_{\mathrm{SNO}}^{\mathrm{th}}}. \qquad (3)$$

3. Results

In order to clarify the role played by epitaxial strain on the transport properties of the SNO films, we carried out resistivity and strain measurements for two films with the same thickness ($t = 17$ nm), one deposited on STO (sample 1) and the other on LAO (sample 2). The respective resistivity measurements plotted versus temperature are displayed in figure 1(a) (open circles correspond to experimental data). The film deposited on LAO (curve (1) figure 1(a)) clearly shows a sharp MI transition whereas the MI transition is strongly flattened as SNO is deposited on STO (curve (3) figure 1(a)). Furthermore the resistivity is two orders of magnitude higher in the latter

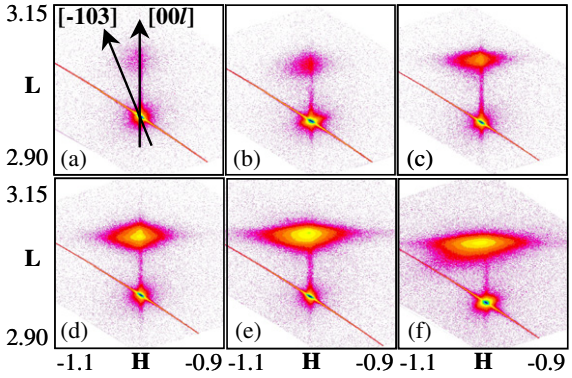

Figure 2. ($\bar{1}03$) RSMs of SNO films deposited on STO with thickness 17 nm (a), 22 nm (b), 38 nm (c), 85 nm (d), 150 nm (e) and 500 nm (f). The intense peak located at $(H, L) = (-1, 3)$ is the substrate peak whereas the broader peak is the ($\bar{1}03$) reflection of the film.

case. These measurements simply indicate that the change of substrate and hence the change of misfit sign strongly affects the resistivity behavior of the SNO films. We propose to elucidate the strain–resistivity relationship with the help of structural and microstructural investigations involving strain state measurements. In this goal, we evaluated the strained lattice parameters of the two films. For sample 1 we recorded a ($\bar{1}03$) RSM (figure 2(a)). From the relative position of the SNO ($\bar{1}03$) reciprocal lattice point (RLP) with respect to the position of the STO ($\bar{1}03$) RLP we calculated $a_{\parallel}$ and $a_{\perp}$ and obtained $a_{\parallel} = 3.903$ Å and $a_{\perp} = 3.845$ Å (the uncertainty is 10^{-4} Å). $a_{\parallel}$ is almost equal to a_{STO} which evidences that the SNO film is highly strained on the STO substrate. Contrarily to what is expected $a_{\perp}$ is much higher than the value of the bulk (i.e. strain-free) SNO lattice parameter. Actually, the lattice parameter of STO being larger than those of bulk SNO, the SNO film is then subjected to in-plane tensile strain which should involve an out-of-plane contraction instead of the observed expansion. This unexpected result suggests that the actual lattice parameter of SNO, a_{SNO}, must be higher than its commonly assumed value $a_{\mathrm{SNO}}^{\mathrm{th}}$. In other words, the SNO film undergoes chemical relaxation. To confirm this statement we calculated the actual lattice parameter, the mechanical and chemical strain relaxation rates and obtained $a_{\mathrm{SNO}} = 3.868$ Å, $R_{\mathrm{m}} = 5.4\%$ and $R_{\mathrm{c}} = 66.4\%$. This means that the SNO film is highly chemically relaxed. High values of a_{SNO} have already been observed in bulk $RNiO_3$ compounds and result from the formation of oxygen vacancies during the synthesis [14, 15]. Nikulin *et al* reported in [14] the increase of the unit cell volume of bulk $RNiO_{3-\delta}$ (R = Nd, Sm) compounds as δ increases. We postulate that similarly to what happens in $CaRuO_3$ compounds [26], the formation of oxygen vacancies occurs from the destabilization of the transition metal ion, here Ni^{3+}, which turns into Ni^{2+}. Because the latter has a larger ionic radius the lattice parameters increase. It is then obvious from the calculation of a_{SNO} of sample 1 that the SNO film contains oxygen vacancies.

For sample 2, due to the well-known twinned structure of the LAO crystal, a splitting of the RLPs of LAO and SNO

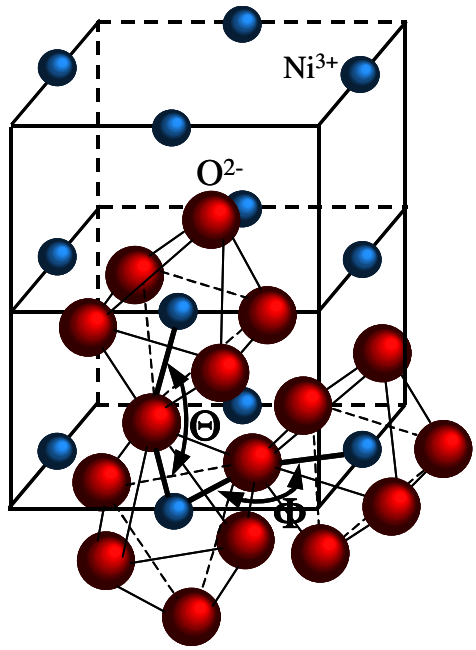

Figure 3. Scheme of the orthorhombically distorted perovskite structure. Φ and Θ (the in-plane and out-of-plane Ni–O–Ni bond angles) parametrize the lattice distortion of the $RNiO_3$ structure and are related to the lattice parameters $a_{\parallel}$ and $a_{\perp}$ through empirical relations.

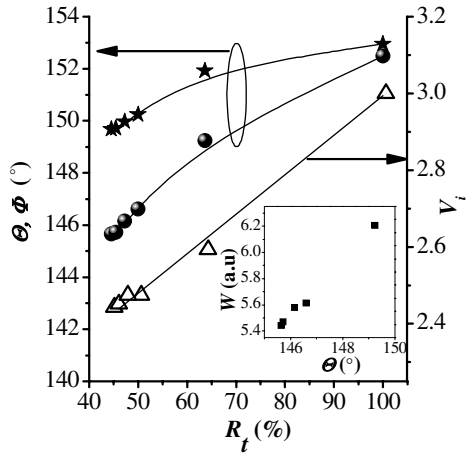

Figure 4. Plot of the Ni–O–Ni bond angles (left axis), Φ (filled stars) and Θ (filled circles) and the valence of the nickel V_i (right axis, open triangles) versus R_t. The lines are guides for the eyes. The Ni–O–Ni bond angles straighten as the strain relaxation increases due to the reduction of the NiO_6 octahedra tilting. The in-plane tensile strain tends to destabilize Ni^{3+} which transforms into Ni^{2+} and gives rise to the formation of oxygen vacancies. Inset: plot of the bandwidth of the transition metal W versus Θ, W increases with Θ (and hence with the strain relaxation) which implies a decrease with Θ of the charge-transfer gap between the occupied oxygen 2p valence band and the unoccupied nickel 3d conduction band.

arises that prevents us from using the asymmetrical RSMs to extract the strained lattice parameters of SNO. We derived $a_{\perp}$ from a (002) L scan and obtained $a_{\perp} = 3.849$ Å. On LAO, the SNO film is subjected to in-plane compressive strain, hence this gives rise to an out-of-plane expansion of the lattice parameter. The measured value of $a_{\perp}$ is much higher than $a^{\text{th}}_{\text{SNO}}$ which evidences the high state of strain of the SNO film on LAO. When SNO is deposited on STO, the in-plane expansion of the NiO_6 octahedra is energetically unfavorable because of the small size of the Ni^{3+} ion located at the center. The tensile strain leads then to the change in oxidation state of the nickel from Ni^{3+} to Ni^{2+} involving an out-of-plane expansion (Ni^{2+} being bigger than Ni^{3+}) instead of the expected contraction. This phenomenon is accompanied by the formation of oxygen vacancies for charge conservation. In turn, because the lattice parameter of LAO is lower than the lattice parameter of bulk SNO, the in-plane compressive strain arising at the SNO/LAO interface stabilizes the Ni^{3+} by reducing the volume of the octahedral cavity.

4. Discussion

4.1. Strain-induced structural changes

In order to understand the observed flattened resistivity curves obtained for the SNO films deposited on STO, we performed structural measurements on these SNO films with different thicknesses (from $t = 22$ to 500 nm).

The distortion of the $RNiO_3$ structure is usually defined with the tolerance factor. A change in the tolerance factor can be associated with a change in either or both of the bond lengths d(R–O) and d(Ni–O). Another way of parametrizing the lattice distortion of this structure is to use the Ni–O–Ni bond angles. The orthorhombic perovskite structure is represented schematically in figure 3 where Φ and Θ are the in-plane and out-of-plane Ni–O–Ni bond angles. Hayashi *et al* [27] derived empirical relations between Ni–O–Ni bond angles and lattice parameters. We used the relations given in [27] to derive Φ and Θ.

Furthermore, we used the bond valence method to evaluate the valence of Ni in these films [28]. This method relies on an empirical expression between the bond length d_{ij} and the valence of a bond v_{ij} between two atoms i and j [29–31]. Finally, the valence V_i of an atom i is defined as the sum of all the bond valences v_{ij}. Calculation of Φ, Θ and V_i as a function of the total strain relaxation rate R_t (equation (3)) are obtained from the measurement of $a_{\parallel}$ and $a_{\perp}$ using the $(\bar{1}03)$ RSMs (figures 2(b)–(f)). Results are displayed in figure 4. Values for $R_t = 100\%$ correspond to the values obtained for bulk $SmNiO_3$ that can be found in the literature [27]. Figure 4 clearly shows an increase of the Ni–O–Ni bond angles as the strain relaxation increases. Indeed, the tilting of the NiO_6 octahedra is due to a mismatch between the rare-earth size and the free space between the corner-sharing octahedra: the rare-earth are too small to fill this space, therefore causing the NiO_6 octahedra to tilt in order to decrease the free space. The tensile strain generated at the interface by the STO substrate amplifies this phenomenon resulting in an increase of the NiO_6 octahedra's tilting and a closing of the Ni–O–Ni bond angles as compared to the 180° angle of the ideal perovskite structure. This picture is supported by works examining the pressure or the strain relaxation dependence of the MI transition in bulk $RNiO_3$ (R = Pr, Nd) and in LSMO thin films [7, 8, 32, 33].

Figure 4 also shows that the valence of the nickel, V_i, increases with R_t. The in-plane tensile strain tends to destabilize Ni^{3+} which transforms into Ni^{2+} and gives rise to the formation of oxygen vacancies for charge conservation (as postulated in section 3).

We would like now to focus on the strain dependence of the MI transition temperature in $RNiO_3$ and its importance from the point of view of the electronic structure of these materials. This requires careful considerations relative to the steric effects existing in these orthorhombic perovskites when the temperature, the rare-earth size, or the strain are modified. The structure of the orthorhombically distorted perovskites was analyzed by O'Keeffe *et al* [34] and Hayashi *et al* [27] who evidenced the existence of simple relations between the lattice parameters, the ionic radius of the rare-earth and Ni cations, and the Ni–O–Ni bond angles. Since the MI temperature is known to depend on the tolerance factor [1], it can be expected that T_{MI} is directly dependent on the Ni–O–Ni bond angles. The identification of the physical mechanism of the transition in $RNiO_3$ is taken from a broad study [1, 4, 9, 35] that relies on the ZSA (Zaanen, Sawatzky and Allen) model [5, 36]. This model has been shown to be able to account for the differences between metallic and insulating behavior for a wide range of oxides. Later, Torrance *et al* showed that $RNiO_3$ compounds belong to the charge transfer type [35]. In the charge transfer gap framework outlined by Torrance *et al*, the gap between the occupied oxygen 2p valence band and the unoccupied nickel 3d conduction band is reduced as the bandwidth of the transition metal W is increased, eventually going to zero as the valence and conduction bands overlap, giving rise to the metallic state. The fact that the bandwidth may be increased by either the temperature or the rare-earth size is clearly related to the degree of orthorhombicity, i.e the values of the Ni–O–Ni bond angles [32]:

$$W = \cos w/(d_{\mathrm{Ni-O}})^{3.5} \qquad \text{with } w = 2\pi - \langle \mathrm{Ni\text{–}O\text{–}Ni} \rangle . \tag{4}$$

Many studies performed on bulk $RNiO_3$ compounds indeed showed that T_{MI} decreases as the Ni–O–Ni bond angles increases [7, 8]. The inset in figure 4 shows that the strain relaxation acts on the Ni–O–Ni bond angles similarly to the temperature or the rare-earth size, i.e. it increases W (calculated from equation (4)). Hence, high values of T_{MI} should be expected (as compared to the bulk value $T_{MI} = 130\,^{\circ}\mathrm{C}$) for the thinner SNO films.

4.2. Role of strain on the transport properties

Previous HRXRD investigations on the SNO films deposited on STO evidenced the existence of a strain gradient within the films [21]. The strain profile (figure 5(a)) has been retrieved by the simulation of the (00l) L scans of the films using a model described in details elsewhere [19]. Figure 5(b) shows the simulation of a (002) L scan. It can be seen that the tensile strain effect due to the creation of oxygen vacancies is more pronounced very close to the SNO/STO interface ($e_{zz} = 2.8\%$). Between 4 nm and the surface, the strain profile exhibits oscillations and it is to date not clear whether these oscillations have a physical meaning. However, it is clear

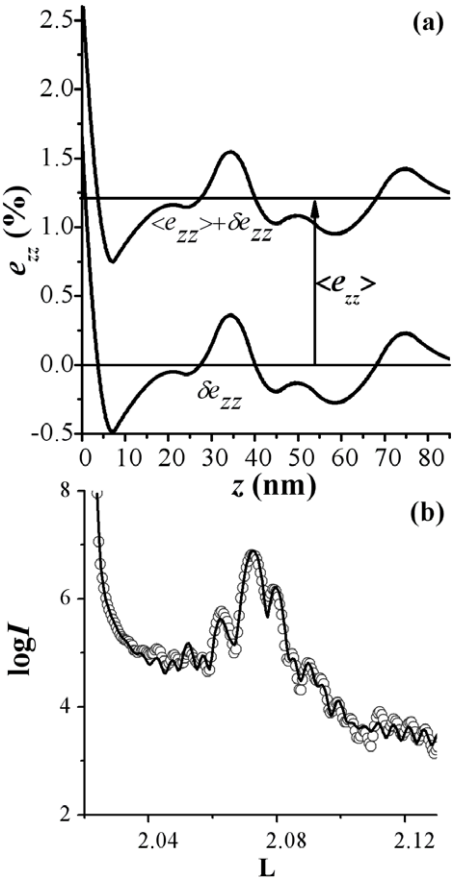

Figure 5. (a) Plot of the strain e_{zz} versus z of the 85 nm thick SNO film deposited on STO, the effect of oxygen vacancies is more pronounced at $z = 0$ where the interface is tensily strained. (b) (002) L scan of the 85 nm thick SNO film deposited on STO (circles: data, line: simulation), the simulation of the (002) L scan allowed us to retrieve the strain profile e_{zz}.

that the film is not homogeneously strained and that the strain progressively decreases when moving from the interface to the surface. Let us first consider the effect of inhomogeneous strain (δe_{zz}). In order to describe the effect of this strain gradient on the transport properties we suggest to divide the films into lamellas, each lamella having a constant strain value and hence a constant T_{MI} value. We therefore simulated the resistivity curves of the SNO films using the model proposed by Catalan *et al* [9] in which the semi-conducting state ($T < T_{MI}$) can be described by assuming a combination of two transport mechanisms acting simultaneously throughout the entire temperature range: the variable range hopping mechanism and the activated behavior [9]:

$$\sigma_i = 1/R_i = A\exp(-B/T^{1/4}) + C\exp(-D/T). \tag{5}$$

σ_i is the conductivity in one single lamella of the film, A, B, C and D are constants. Besides, the conductivity of the metallic state ($T > T_{MI}$) is easily described by a straight line. Equation (5) allowed us to fit properly the resistivity behavior of the SNO film deposited on LAO (curve 1 in figure 1(a)) and so to determine the constants A, B, C and D. In the scheme proposed here the conductances act in parallel so that for the

SNO film deposited on STO it comes:

$$\sigma_{\text{film}} = \sum_i \sigma_i . \tag{6}$$

The resulting resistivity profile obtained from equations (5) and (6) (considering that the film is divided into 20 lamellas) corresponds to the curve 2 in figure 1(a). It turns out that the distribution of T_{MI} across the film thickness due to δe_{zz} result in a strong flattening of the resistivity curve (curve 2, figure 1(a)). However, the calculated resistivity curve is two orders of magnitude below the actual SNO/STO curve. This discrepancy can be explained by the fact that the conductivity parameters (A, B, C, D) are those corresponding to SNO deposited on LAO, whereas one should consider here the conductivity of SNO deposited on STO, i.e. one should take into account the average state of strain of the film $\langle e_{zz} \rangle$. As mentioned in the previous section, this strain mainly results from the presence of Ni^{2+} and oxygen vacancies. We argue that the presence of Ni^{2+} and oxygen vacancies can be associated to an increase of the charge transfer gap, i.e. the conductivity of each curve is reduced to σ_i / k, where k is a constant. The introduction of this single parameter allows us to fit the experimental curve over the entire temperature range (curve 3, figure 1(a)). Figure 1(b) corresponds to the curve 3 plotted in the temperature range 30–500 °C, it clearly evidences a MI transition at $T_{\text{MI}} = 400$ °C instead of 130 °C (for bulk $SmNiO_3$). This simulation proves that a strain gradient induces a shift of T_{MI} towards high values of temperature then stabilizing the semi-conducting state over the metallic state in the temperature range 30–400 °C and flattens the resistivity curve in the semi-conducting temperature range.

5. Conclusion

In the foregoing text, an accurate study devoted to clarify the correlation between the strain state and the MI transition of epitaxial $SmNiO_3$ films is reported. In the first part, the role of epitaxial strain on the stabilization of Ni^{3+} is evidenced. Indeed, we proved via misfit strain measurements and valence bond calculations that an in-plane compressive strain stabilizes the 3+ oxidation state of the nickel whereas an in-plane tensile strain induces a progressive change in oxidation state from Ni^{3+} to Ni^{2+} that leads to the formation of oxygen vacancies very close to the SNO/STO interface. In the second part, a careful attention is paid to the evolution of the orthorhombic lattice distortion of the SNO films deposited on STO as a function of the strain relaxation. This distortion is assessed in terms of Ni–O–Ni bond angles. As expected from previous studies performed on bulk $RNiO_3$, it turns out that the relaxation of in-plane strain induces a straightening of the Ni–O–Ni bond angles. Here, the strain relaxation acts as the temperature or the rare-earth size on the Ni–O–Ni bond angles and therefore provides a powerful tool to tune the MI transition temperature as the Ni–O–Ni bond angles are related to the bandwidth of the transition metal. Finally, we have shown that the strain has a huge influence on the transport properties of the SNO films. Compressive strain (SNO/LAO) stabilizes Ni^{3+} so that the films exhibit a marked MI transition at 120 °C. Conversely, tensile strain (SNO/STO) destabilizes Ni^{3+} so that the films are much more resistive and exhibit a flat resistivity curve. The flattening of the resistivity curve can be understood by taking into account the inhomogeneous strain distribution across the film thickness, whereas the increase of resistivity has been ascribed to the homogeneous part of the strain.

Acknowledgment

The authors express their thanks to the FAME European Network of Excellence for financial support.

References

[1] Torrance J B, Lacorre P, Nazzal A I, Ansaldo E J and Niedermayer Ch 1992 *Phys. Rev.* B **45** 8209
[2] Lacorre P, Torrance J B, Pannetier J, Nazzal A I, Wang P W and Huang T C 1991 *J. Solid State Chem.* **91** 225
[3] Medarde M L 1997 *J. Phys.: Condens. Matter* **9** 1679
[4] García-Muñoz J L, Rodríguez-Carvajal J, Lacorre P and Torrance J B 1992 *Phys. Rev.* B **46** 4414
[5] Zaanen J, Sawatzky G A and Allen J W 1985 *Phys. Rev. Lett.* **55** 418
[6] Alonso J A, Martínez-Lope M J, Casais M T, García-Muñoz J L, Fernández-Díaz M T and Aranda M A G 2001 *Phys. Rev.* B **64** 094102
[7] Canfield P C, Thompson J D, Cheong S W and Rupp L W 1993 *Phys. Rev.* B **47** 12357
[8] Obradors X, Paulius L M, Maple M B, Torrance J B, Nazzal A I, Fontberta J and Granados X 1993 *Phys. Rev.* B **47** 12353
[9] Catalan G, Bowman R M and Gregg J M 2000 *Phys. Rev.* B **62** 7892
[10] Gorbenko O Yu, Novojilov M A, Graboy I E, Amelichev V A, Bosak A A, Nikulin I V, Kaul A R, Guettler B, Wahl G, Babushkina N A, Belova L M and Zandbergen H W 2001 *Int. J. Inorg. Mater.* **3** 1303
[11] Kim S J, Demazeau G, Alonso J A, Largeteau A, Presniakov I and Choy J H 2001 *Solid State Commun.* **117** 113
[12] Demazeau G, Marboeuf A, Pouchard M and Hagenmuller P 1971 *J. Solid State Chem.* **3** 582
[13] Demazeau G 2005 *Z. Anorg. Allg. Chem.* **631** 556
[14] Nikulin I V, Novojilov M A, Kaul A R, Mudretsova S N and Kondrashov S V 2004 *Mater. Res. Bull.* **39** 775
[15] Tiwari A and Rajeev K P 1999 *Solid State Commun.* **109** 119
[16] Mahesh R, Kannan K R and Rao C N R 1995 *J. Solid State Chem.* **114** 294
[17] Ihzaz N, Pignard S, Kreisel J, Vincent H, Marcus J, Dhahri J and Oumezzine M 2004 *Phys. Status Solidi* c **1** 1679
[18] Conchon F, Boulle A, Girardot C, Pignard S, Guinebretière R, Dooryhée E, Hodeau J L, Weiss F, Kreisel J and Bérar J F 2007 *J. Phys. D: Appl. Phys.* **40** 4872
[19] Boulle A, Guinebretière R and Dauger A 2005 *J. Appl. Phys.* **97** 073503
Boulle A, Masson O, Guinebretière R and Dauger A 2003 *J. Appl. Crystallogr.* **36** 1424
[20] Boulle A, Guinebretière R and Dauger A 2005 *J. Phys. D: Appl. Phys.* **38** 3907
[21] Conchon F, Boulle A, Girardot C, Pignard S, Guinebretière R, Dooryhée E, Hodeau J L, Weiss F and Kreisel J 2007 *Mater. Sci. Eng.* B **144** 32

[22] Boulle A, Masson O, Guinebretière R, Lecomte A and Dauger A 2002 *J. Appl. Crystallogr.* **35** 606
[23] Ferrer J L, Simon J P, Bérar J F, Caillot B, Fanchon E, Kaïkati O, Arnaud S, Guidotti M, Pirocchi M and Roth M 1998 *J. Synchrotron Radiat.* **5** 1346
[24] Dunstan D J 1997 *J. Mater. Sci. Mater. Electron.* **8** 337
[25] Heinke H, Möller M O, Hommel D and Landwehr G 1994 *J. Cryst. Growth* **135** 41
[26] Rao R A, Gan Q, Eom C B, Cava R J, Suzuki Y, Krajewski J J, Gausepohl S C and Lee M 1997 *Appl. Phys. Lett.* **70** 22
[27] Hayashi K, Demazeau G and Pouchard M 1981 *Rev. Chim. Minérale* **18** 148
[28] Brese N E and O'Keeffe M 1991 *Acta Crystallogr.* B **47** 192
[29] Demazeau G, Marboeuf A, Pouchard M and Hagenmuller P 1971 *J. Solid State Chem.* **3** 582
[30] Wilchainchai A, Dordor P, Doumerc J P, Marquestaut E, Pouchard M and Hagenmuller P 1988 *J. Solid State Chem.* **74** 126
[31] Demazeau G, Pouchard M and Hagenmuller P 1976 *J. Solid State Chem.* **18** 159
[32] Zhou J S, Goodenough J B and Dabrowski B 2005 *Phys. Rev. Lett.* **95** 127204
[33] Chen Y H and Wu T B 2007 *Electrochem. Solid-State Lett.* **10** 29
[34] O'Keeffe M, Hyde B G and Boven J O 1979 *Phys. Chem. Minerals* **4** 299
[35] Torrance J B, Lacorre P, Asavaroengchai C and Metzger R M 1991 *J. Solid State Chem.* **90** 168
[36] Zaanen J and Sawatzky G A 1990 *J. Solid State Chem.* **88** 8